INVITED PAPER *Special Section on Microwave and Millimeter-Wave Technologies*

Specificity Analysis for Nonlinear Distorted Radiation Using 4.65 GHz Band Massive Element Active Antenna System for 5G and Influence on Spatial Multiplexing Performance

Takuji MOCHIZUKI[†a)], ***Member***

SUMMARY This paper reports the evaluation and simulated results of the nonlinear characteristics of the 4.65GHz Active Antenna System (AAS) for 5G mobile communication systems. The antenna element is composed of ±45° dual polarization shared patch antenna, and is equipped with total 64 elements with horizontal 8 × vertical 4 × 2 polarization configuration. A 32-element transceiver circuit was mounted on the back side of the antenna printed circuit board. With the above circuit configuration, a full digital beamforming method has been adopted that can realize high frequency utilization efficiency by using the Sub6GHz-band massive element AAS, and excellent spatial multiplexing performance by Massive MIMO has been pursued. However, it was found that the Downlink (DL) SINR (Signal to Interference and Noise Ratio) to each terminal deteriorated because of the nonlinear distorted radiation as the transmission output power was increased in the maximum rated direction. Therefore, it has been confirmed that the spatial multiplexing performance in the high output power region is significantly improved by installing DPD. In order to clarify the affection of nonlinear distorted radiation on spatial multiplexing performance, the radiation patterns were measured using OFDM signal (subcarrier spacing 60kHz × 1500 subcarriers in 90MHz bandwidth) in an anechoic chamber. And by the simulated analysis for the affection of nonlinear distortion on null characteristic, the accuracy of nulls generated in each user terminal direction does not depend on the degree of nonlinearity, but is affected by the residual amplitude and phase variation among all transmitters and receivers after calibration (CAL). Therefore, it was clarified that the double compensation configuration of DPD and high-precision CAL is effective for achieving excellent Massive MIMO performance. This paper is based on the IEICE Japanese Transactions on Communications (Vol.J102-B, No.11, pp.816–824, Nov. 2019).

key words: *5G, AAS, Massive MIMO, DPD, CAL*

1. Introduction

As opposed to the deployment of millimeter-wave system in 5th generation mobile communication (5G), in the frequency range of 6GHz or less, it is not easy to secure the wide frequency bandwidth, but it is necessary to consider that wide area propagation and transmission including non-line-of-sight are possible. Taking these factors into consideration, it is effective in realizing spatial multiplexing and Massive MIMO by AAS which adopts a full digital beamforming method that can realize high frequency utilization efficiency [1], [2].

Therefore, the authors have also developed 5.2GHz band and 4.65GHz band AAS since 2016, but as the transmitted output is increased toward the maximum rated level, it has become clear that DL SINR of the radiated signal for each spatially multiplexed user terminal is significantly degraded.

Furthermore, it was suggested that the interference radiation "I", which determines the DL SINR deterioration at high output, is mainly composed of the nonlinear distortion component generated in the transmitter and has the specificity which is radiated in the same direction as each user terminal. Therefore, it was considered to achieve better transmission performance without giving nonlinear distortion deterioration to DL SINR by setting a low output, but the transmission distance and coverage were significantly reduced, and the characteristics of wide area at 6GHz or less was lost, so it is necessary to improve the nonlinear distortion of the transmitter [3].

Consequently, we have developed a 4.65GHz band AAS equipped with a distortion compensation function by DPD for all 32 transmitters in the AAS, and by implementing nonlinear distortion improvement and a full digital beamforming together, it was confirmed that the spatial multiplexing performance was significantly improved in the high output power region [4].

As the AAS ACLR specified in 3GPP TS38.104 of 5G compliant, since 10Log (NTXU,countedpercell 8)=9dB as the scaling factor (refer to 6.6.3.4 Minimum requirement for BS type 1-H, max. 8 is allowed as NTXU,countedpercell in the case of 32TRX) can be applied for the absolute value ALCR specification of −13dBm/MHz in case of Category A Wide Area BS, so ACLR only needs to satisfy D/U (Desire/Undesire) ratio of 33dBc or more, that can be allowed to apply as less stringent specification from the relative D/U spec. of 45dBc under the each TX output when 1-H BS type is declared. Furthermore, EVM specification of 3.5% (29dBc) for 256QAM is looser than ACLR spec. of 33dBc. Even if these 3GPP specifications are satisfied, a clear standard for spatial multiplexing performance has not been yet determined in 3GPP. However, TX nonlinear distortion becomes a problem when using MU-MIMO to increase the number of spatial multiplexing. Since the nonlinear affection of DL SINR for each terminal is improved by the DPD and CAL performance in AAS, it shall be essential not only to meet the distortion-related standards of 3GPP, but also to understand the affections of nonlinear distorted radiation during spatial multiplexing.

Manuscript received January 18, 2021.
Manuscript revised March 1, 2021.
Manuscript publicized April 8, 2021.
[†]The author is with NEC, Kawasaki-shi, 211–8666 Japan.
a) E-mail: takuji119@nec.com
DOI: 10.1587/transele.2021MMI0007

The fact that the nonlinear distortion of the AAS transmitter generated in the high output power level affects the ACLR (Adjacent Channel Leakage power Ratio) and EVM (Error Vector Magnitude) of the main beam has already been presented as the AAS which adopted the digital beamforming [5]–[12] and the analog beamforming scheme [13]–[17], or as the problem of nonlinear distortion deterioration by the antenna mutual coupling affection for DPD performance [18]–[25]. So, as a problem not analyzed in these papers, the authors have confirmed that nonlinear distortion has a large affection on the spatial multiplexing performance by verifying the peculiarity of nonlinear distorted radiation during multitone transmission represented by OFDM [26].

In this paper, in order to further investigate the deterioration mechanism, multiple OFDM signals are radiated into space in an anechoic chamber, and the opposite reception signal is demodulated or spectrum analyzed to obtain DL SINR and S/I angular spectrum was calculated by S/I separation ("S": Desired wave, "I": Multitone distortion component). By calculating this S/I angular spectrum, the peculiarity of the nonlinear distorted radiation "I" was confirmed, and the peculiarity of the nonlinear strain radiation "I" was also confirmed.

2. Features of 4.65GHz Band Massive Element Active Antenna with DPD Used for the Verification

Figure 1 shows the block diagram of the AAS used for the verification, and Fig. 2 shows the external view of AAS (the photo shows the operation when 2AAS are connected horizontally), and Table 1 shows the specifications of AAS. The antenna element is composed of ±45° dual polarization shared patch antenna, and is equipped with total 64 elements with horizontal 8 x vertical 4 x 2 polarization configuration. As the number of transmitters and receivers (TRXs), we have realized miniaturization with an active antenna configuration in which 32TRXs with horizontal 8 x vertical 2 x 2 polarization are integrally mounted on the back side of the antenna by connecting 2 vertical elements to 1TRX. As a −45° polarization feeding method, 2 feedlines branched from another TRX are connected from the direction orthogonal to the +45° polarization feeding point. And forced air cooling is used as the heat dissipation method for this AAS.

The DPD is individually mounted in the digital baseband section of each transmitter, and distortion compensation is performed by extracting the amplifier (AMP) output with nonlinearity using a directional coupler and returning it to each DPD section. The operation class of the AMP is class AB (GaAs device), and the Generalized Memory Polynomial (GMP) method was adopted as the DPD in order to realize optimum distortion compensation regardless of the nonlinearity of the AMP, also under taking into account the reduction of circuit scale. And DPD of the main signal with 100MHz bandwidth is executed mainly up to the third-order intermodulation distortion as the compensation band within fc ±150MHz. Furthermore, in order to perform uplink channel sounding and downlink beamforming with high accuracy, DL/UL CAL circuit that automatically corrects variations in amplitude and phase frequency characteristics among all 32TRXs is equipped outside of the DPD feedback circuitry, and the linearization of each transmitter in the high output power region is performed by DPD, so the double compensation configuration is applied to correct remaining amplitude and phase variation among all the transmitters with DPD and DL CAL.

It should be noted that the variation of each transmitter/ receiver to RF BPF is subject to the sequentially automatic CAL and is compensated for unification, but since the antenna part is considered as a passive circuit, so it is sufficient to apply fixed variation correction between each

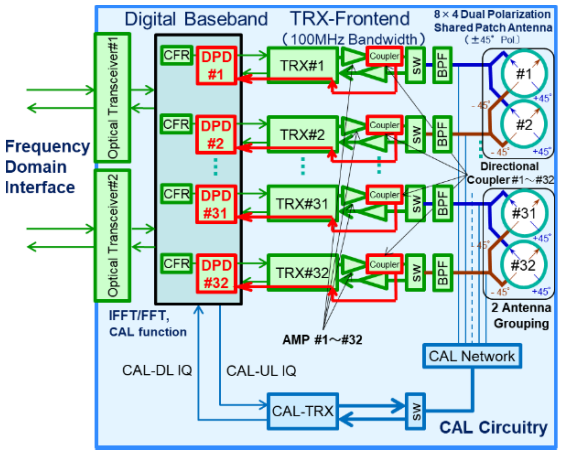

Fig. 1 AAS block diagram.

Fig. 2 AAS external view.

Table 1 AAS specifications.

Frequency	4.65GHz±150MHz (Occupied BW 100MHz)
Subcarrier spacing	60kHz
Antenna element	H8×V4×2 Orthogonal polarization
Antenna element spacing	H:0.52 λ , V:0.61 λ
Antenna beam gain	20.4dBi
Total conducted power (both polarization)	+28dBm
EIRP	+48.4dBm
Each transmitter output	+13.9dBm
External dimensions, volume / weight	287mm(W)×350mm(H)×52～83mm(D), 8.5 Liter / 7kg

antenna. Therefore, by storing the inter-antenna variation correction value in the AAS at the time of shipment from the factory, CAL correction can be completed for all variations by finally adding fixed inter-antenna correction to each transmitter/receiver CAL correction value because of the sequential automatic CAL during TRX operation.

In the verification of the affection of nonlinear distortion in the high output power region on spatial multiplexing performance, which is described later in Chapter 3, the experiments were carried out by switching DPD on/off operation respectively, and especially when DPD is set to off, DL radiation was performed in nonlinear condition without distortion compensation by setting DPD to bypass mode. Due to the above mentioned setting, the affection of the nonlinear distortion itself was confirmed precisely. The importance of the AAS CAL function itself has been already explained in some papers [27]–[29].

3. Verification for the Specificity of Nonlinear Distorted Radiation Generated under OFDM / Single Layer Beam Radiation in the High Output Power Region

With the 4.65GHz band AAS equipped with DPD, the OFDM signal (subcarrier spacing 60kHz× 1500 subcarriers =occupied bandwidth 90MHz) is firstly radiated to the front direction in the anechoic chamber when the nonlinear distortion compensation by DPD is On and Off respectively.

In this analysis, as shown by CCDF (Complementary Cumulative Distribution Function) of PAPR (Peak to Average Ratio) in Fig. 3, by limiting the peak absolute power level 5.2dB/7.2dB/9.2dB higher than the maximum rated output power level (1TX conducted output level: +13.9dBm, single polarization total conducted output level:+25dBm) by CFR (Crest Factor Reduction), a pseudo-nonlinear characteristic is set in the AAS so that the peak power of the OFDM signal passing through each TX system is intentionally clipped. Hereafter, the same absolute power level limitation is abbreviated as "CFR setting 5.2dB" or "CFR=5.2dB". The saturation level of TX AMP exists above the maximum rated output power +9.2dB.

The output level dependency of DL SINR measured in anechoic chamber is summarized in Fig. 4, by converting the RF signal received by the receive side vertically polarized antenna and vector signal analyzer to the I/Q digital baseband signals and performing demodulation analysis.

Due to Fig. 4, it can be clarified that DPD improves the amplitude and phase linearity of each TX arm until a remarkable nonlinear distortion occurs in the peak clipping defined in each CFR setting.

Then for each DPD On/Off case, the same OFDM signal is radiated to the front direction in the anechoic chamber as a single layer beam, and the angular spectrum of the desired signal "S" was obtained by taking the cross-correlation between the received signal.

Furthermore, by subtracting the desired signal "S" from the total received signal of each horizontal angle, the

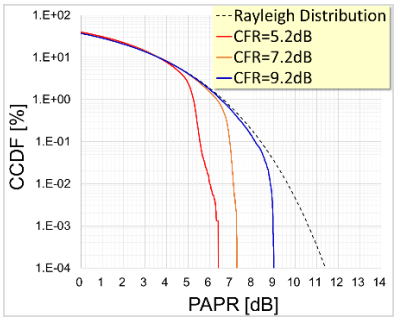

Fig. 3 PAPR characteristics at CFR setting 5.2dB/7.2dB/9.2dB

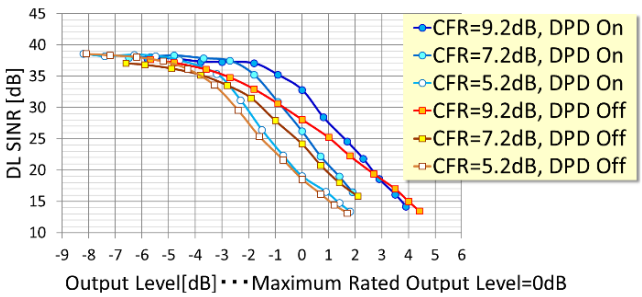

Fig. 4 Output level vs. DL SINR at single layer beam in each CFR

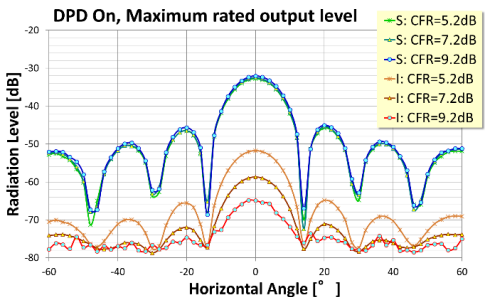

Fig. 5 S/I angular spectrum with DPD On in each CFR setting

interference signal "I", which is mainly determined by the nonlinear distortion at high output power region, was separated and the angular spectrum of the nonlinear distorted radiation "I" was obtained.

As a result, Fig. 5 shows the S/I angular spectrum obtained for each of the CFR settings of 5.2dB/7.2dB/9.2dB at the maximum rated output power when DPD is On, the same S/I angular spectrum when DPD is Off is summarized in Fig. 6.

In Fig. 5 and Fig. 6, the radiation specificity of the component "I" consisting of the multitone distortion under the OFDM transmission was actually measured and verified, and it was confirmed that the component "I" was emitted in the same direction as the desired radiation "S" [16].

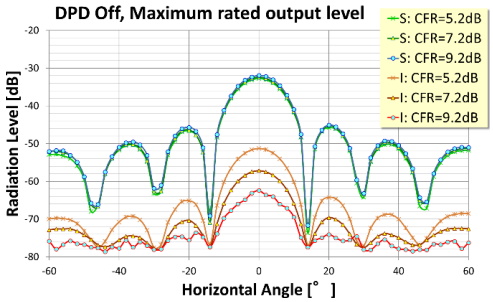

Fig. 6 S/I angular spectrum with DPD Off in each CFR setting

4. Verification for the Specificity of Nonlinear Distorted Radiation Generated under OFDM / Multi-Layer Beam Radiation in the High Output Power Region

Furthermore, in order to clarify the radiation specificity of the nonlinear distortion component under the spatial multiplex radiation with multiple layer beams by OFDM/ multitone in the high output power region, the NPR (Noise Power Ratio) method shown in Fig. 7 was applied [30], [31]. And Notch Out Band with the several subcarriers turned off was set in the OFDM frequency band (the center frequency is 4.55GHz with subcarrier spacing 60kHz× 1500 subcarriers, so all 125 Physical Resource Blocks are occupied in ±45MHz bandwidth) under the DPD operation is On and Off. Moreover, when multiple layer beams are multiplexed in the desired wave "S" (140 subcarriers for 95 Physical Resource Blocks) outside of the Notch Out Band (Notch Out 30 Physical Resource Blocks 21.6MHz width from 4561.88MHz to 4583.48MHz), the radiation characteristics as its direction and level for the spatially multiplexed component "S" in the horizontal direction (Front 0° radiation for 1 layer beam, 0° and −20° radiation for 2 layer beams, 0°, −20°, +20° and −40° radiation for 4 layer beams) and the multitone distortion component "I" that falls into the Notch Out Band were measured using spectrum analyzer set up at opposite side of AAS in the anechoic chamber in order to verify the dependency for the radiation direction and level between "S" and "I".

The "S" and "I" radiation levels were individually measured in the 5MHz bandwidth, and DL SINR was measured as an alternative to the D/U ratio of the "S" and "I" levels. And the peak power limitation was fixed as CFR setting of 9.2dB.

The NPR method used with this investigation compares the D/U ratio between the multitone distortion level "I" that drops into the Notch Out Band under the high output level operation and the desired wave level "S" in the frequency band where the subcarriers exists outside of the Notch Out Band, and by comparing and actually measuring the D/U ratio in a certain unit bandwidth, it is possible to directly measure the DL SINR caused by the nonlinear distortion that occurs in the OFDM band. Furthermore, since the Notch Out Band where the multitone distortion drops and the desired wave band that radiates the spatial multiplex signal can be discriminated on the frequency domain, so when spatial multiplex radiation is performed, it is effective because the envelope pattern of the desired wave "S" radiated to the multiple directions and also the envelope radiation by the multitone distortion component "I" can be directly measured.

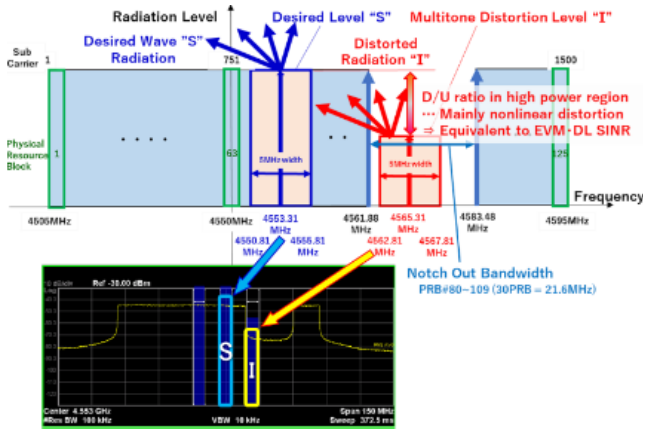

Fig. 7 Frequency spectrum of test signal used for multitone distortion radiation measurement during multi-layer beam radiation by NPR

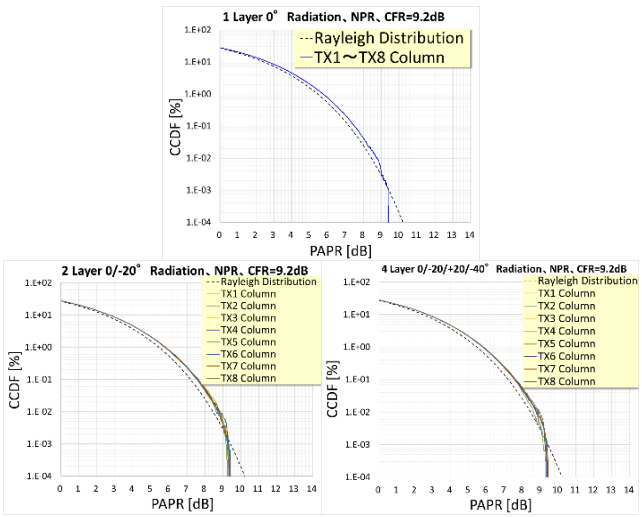

Fig. 8 PAPR characteristics at 1 layer, 2 layer, 4 layer beams radiation

As shown in Fig. 8 in which the PAPR of each of the multiple layer signals multiplexed on the desired wave "S" outside the Notch Out Band is represented by CCDF, as with the spatial multiplexing situation during actual operation, the uncorrelatedness between each layer signal is guaranteed by processing such as scrambling, so it is important that the PAPR as a signal passing through each TX arm is the same regardless of the number of spatial multiplex layer beams of 1/2/4 layer.

Regarding 8TXs in the horizontal direction, since 4TXs (vertical 2TXs × 2 polarization) in each vertical column radiates the same signal, the PAPR in the same column is the same. Therefore, Fig. 8 shows the PAPR for each TX column.

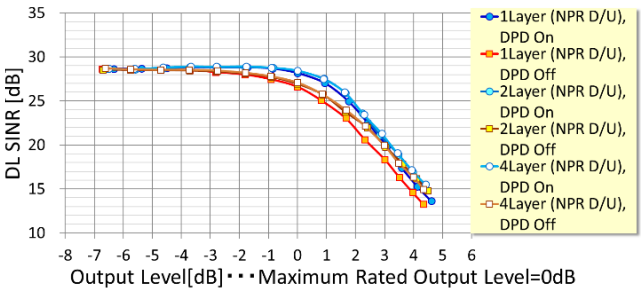

Fig. 9 Output level vs. DL SINR at 1/2/4 layer beams (NPR method)

By using the same NPR method, each output level vs. DL SINR at 1 layer beam radiation, 2 layer beams radiation and 4 layer beams radiation was respectively measured in the anechoic chamber, and these results are summarized in Fig. 9.

In the lower output level region in Fig. 9, since the low distortion level "I" in the Notch Out section is lower than the out-of-band frequency spectrum of a sinc function (SINC spectrum) from the existing OFDM subcarriers, alternative verification for DL DINR by the NPR method is only effective in the higher output power region where distorted radiation is dominant. DL SINR in the lower output power region is dominated by SINC spectrum and asymptotically approaches 29dB.

As described results in Fig. 8, since PAPR of the signal passing through each TX arm is the same among 1/2/4 layer beams regardless of the number of spatial multiplex layer beams, it was confirmed in Fig. 9 that the multitone distorted radiation level and DL SINR appearing in each layer beam direction are almost similar (variation of DL SINR of about 4dBp-p) regardless of the number of multiplexes.

Regarding the degree of nonlinearity exceeding the maximum rated output power level in the investigating condition where the peak level of AMP input signal is increased by CFR 9.2dB from RMS level, DPD effect cannot be expected because the AMP output signal is hard clipped by the saturation level of AMP. Thus, DL SINR converges to the similar value for both DPD On/Off.

As described before, if PAPR of the spatial multiplex signal passing through each transmitter is constant regardless of the number of multiplexes, the degree of nonlinear distortion generation of the transmitter is also the same. Therefore, it was confirmed that DL SINR that arrives to each user terminal after spatial separation has a constant aspect according to the total output level of the spatial multiplex signal passing through each transmitter regardless of the spatial multiplex. And in order to verify the peculiarity of the generated multitone distorted radiation pattern, after setting each TX output to the maximum rated output power +5dB (set to an output level where DL SINR is dominantly determined by nonlinear distortion) for both DPD On/Off case, the angular spectrum of the desired wave "S" and multitone distorted radiation "I" when radiating 2 layer beams $0°/-20°$ and 4 layer beams $0°/-20°$ with the NPR condition are shown in Fig. 10.

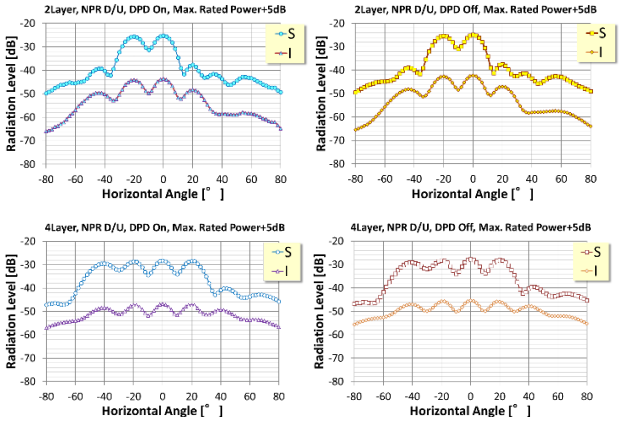

Fig. 10 S/I angular spectrum at 2/4 layer beams radiation (NPR method)

As a result, similar to the radiation aspect of multitone distortion by demodulation analysis in the opposite side of AAS under the 1 layer beam radiation in Fig. 5 and Fig. 6, the multitone distorted radiation "I" is radiated in the same direction as the desired wave "S" of each multi-layer beam.

As mentioned above, since this verification was performed in the strong nonlinear region with the maximum rated output power +5dB, the S/I angular spectrum difference between DPD On/Off is small.

In the multitone distorted radiation "I" pattern when radiating 4 layer beams, the TX/RX level in the anechoic chamber of each 4 layer is divided into 4 equal power level from absolute maximum power level+5dB, so the "I" level that falls into the Notch Out band by NPR method is visible with the noise floor adding of the opposite side spectrum analyzer's RX.

5. Simulated Analysis for the Affection of Nonlinear Distortion on Null Characteristic

In order to confirm the affection regarding the degree of nonlinearity on the null generated for the spatial multiplexing, we used the angular spectrum analysis method in the pseudo-nonlinear state according to each CFR setting in Chapter 3, and in order to further improve the verification accuracy for nonlinear dependency on null characteristic, the following simulation analysis was also performed.

Firstly, the nonlinearity (AM-AM, AM-PM with DPD On/Off) of each TX arm of AAS (TRX-Frontend circuitry including AMP) is modeled by 7th order polynomial approximation from the actual measurement, then each pseudo transmission model was constructed. Figure 11 shows the procedure for extracting and modeling as AM-AM and AM-PM characteristics from the actual nonlinearity of the TRX-Frontend section including each 32 AMP in the AAS.

In step ① of Fig. 11, the same OFDM modulated test signal as the various radiation tests (occupied bandwidth 90MHz) is input from the Digital Part (DP) outside of AAS to the 32TX in AAS (e.g. the case of CFR setting 5.2dB and 9.2dB is respectively represented), and in step ②, the digital signal with peak suppression by each CFR setting in the

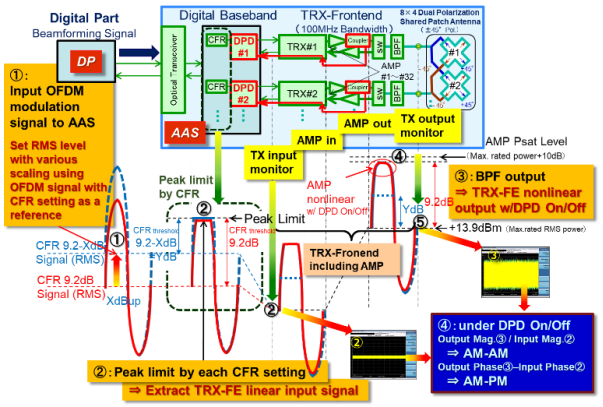

Fig. 11 Nonlinear modeling procedure of TRX-Frontend part

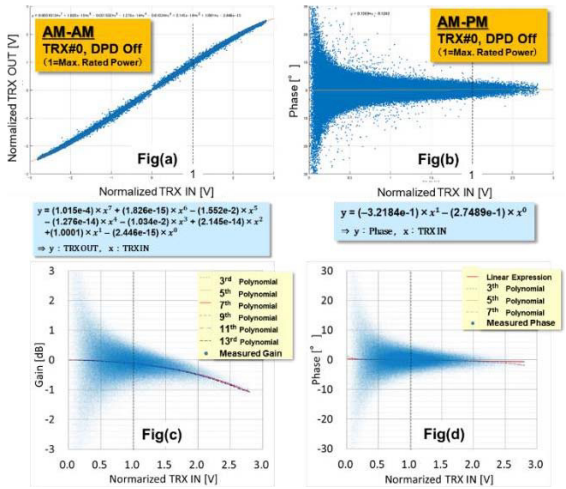

Fig. 12 AM-AM and AM-PM modeling

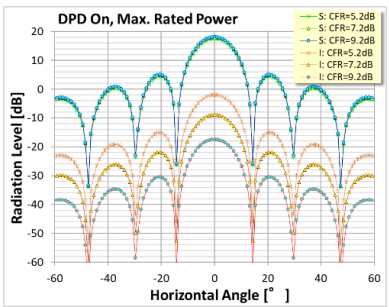

Fig. 13 S/I angular spectrum with DPD On in each CFR (Simulation)

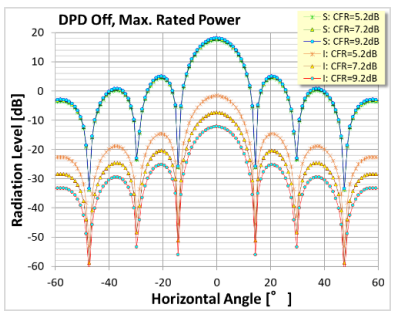

Fig. 14 S/I angular spectrum with DPD Off in each CFR (Simulation)

digital baseband of AAS was extracted and monitored at the outside of AAS.

Regarding the input signal and output signal of the TRX-Frontend section including AMP, firstly the delay of the input and output signal derived by step ③ is adjusted by performing correlation detection, and after synchronizing between the two signals, AM-AM was obtained by dividing the output amplitude ③ by the input amplitude ②, and AM-PM was obtained by subtracting the input phase ② from the output phase ③, as mentioned in step ④.

The upper figure of Fig. 12 shows a representative example of AM-AM (upper left figure (a), true value expression) and AM-PM (upper right figure (b)) obtained from the input and output of the TRX-Frontend section including AMP, and the lower figure of Fig. 12 shows a modeling example by polynomial approximation for both gain and phase (nonlinear modeling is performed separately when DPD is Off as well as when DPD is On). Since AM-AM is a 7th-order polynomial approximation (lower left figure (c), the vertical axis is "Gain") because the difference in model accuracy of 9th order or higher can be ignored, and AM-PM (lower right figure (d)) is a 1st-order approximation and "Phase" fluctuation is assumed regardless of the input level.

Then, single layer beam radiated signal beamformed to the front direction with pseudo-nonlinearity added at each CFR setting similar to the actual measurement is input to the AM-AM/AM-PM modeling that pseudo-expresses the nonlinearity of each TX arm, and after synthesizing the output signal of each TX arm in calculation, the angular spectrum was calculated with arbitrary horizontal angular resolution. And the angular spectrum calculation is the result of considering the radiation pattern characteristics of the antenna element itself.

Firstly, under the maximum rated TX output power setting, the calculation results of the S/I angular spectrum at each CFR setting of 5.2dB/7.2dB/9.2dB with DPD On are shown in Fig. 13, and the calculation results of the S/I angular spectrum performed under the same conditions when DPD is Off are shown in Fig. 14.

As a result, it can be confirmed that the simulated Fig. 13 and Fig. 14 are almost the same as the corresponding measured results and the angular spectrum of Fig. 5 and Fig. 6 respectively. And also as the radiation specificity, it was confirmed that the nonlinear distorted component "I" is radiated in the same direction as the desired wave "S" as same as the actual measurement results.

Furthermore, on the basis of the simulated results in Fig. 13 and Fig. 14, it is shown in Fig. 15 that the SIR by the desired wave "S" and the nonlinear distorted component "I" at each CFR setting is constant regardless of the horizontal angle.

Due to these results, when considering the combined radiation of "S" and "I" which is actually emitted into space, since the "I" increment for "S" level in the desired wave di-

rection and the "I" increment for null level in the direction of the other radiation beams during spatial multiplexing are canceled out when calculating the null depth at the combined radiation of "S"+"I", it can be estimated that the null angle and the null depth are invariant regardless of the degree of nonlinearity.

Therefore, the null accuracy under the spatial multiplexing does not depend on the nonlinearity of each transmitter, and it is possible to maintain the accuracy by minimizing the residual amplitude and phase variation between all transmitters and receivers which are determined by the DL/UL CAL accuracy [4].

The fact that the SIR in each nonlinear condition is constant regardless of the horizontal angle as shown in Fig. 15 coincides with the relative coincidence of the angular spectrum of the desired wave "S" and the nonlinear distorted component "I", these can be explained from the results which are verified by the authors in Ref. [26]. In Ref. [26], the radiation aspect of the double sideband by IM3 (Third-order intermodulation) during spatial multiplex radiation with 2 tones, which is the basis for analyzing multitone distorted radiation (it is necessary to pay attention to IM3 radiation, which is dominant in the nonlinear distortion), was verified by theoretical calculation and actual measurement radiation, and as a result, since the same phase as beamforming weight of the desired wave "S" appears in the phase of IM3 components, the nonlinear distorted radiation "I" is also radiated in the same direction as the desired wave radiation "S", the angular spectrum of the desired wave "S" and the nonlinear distorted component "I" are relatively consistent.

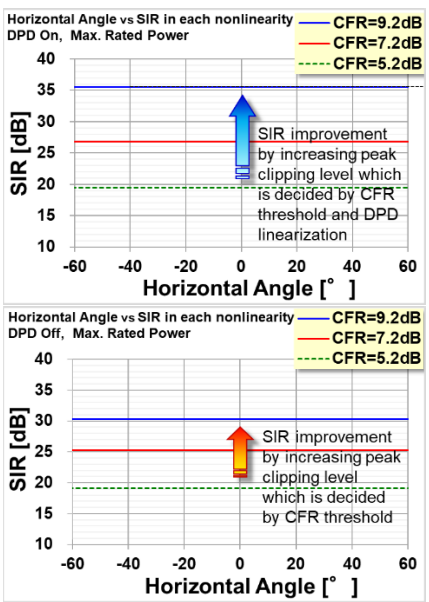

Fig. 15 Horizontal angle dependency of SIR determined by the angular spectrum for the desired wave "S" and nonlinear distortion "I" under CFR setting 9.2dB/7.2dB/5.2dB (Simulation)

6. Impact of Nonlinear Distorted Radiation and Null on Spatial Multiplexing Performance in the High Output Power Region and Improvement Measures for AAS

Although the specificity of multitone distorted radiation and its influence on null formation have been explained above, the level relationship between nonlinear distorted radiation and null in spatial multiplexing and the degree of influence are clarified in this chapter. In order to clarify the level relationship and influence of nonlinear distorted radiation and null in spatial multiplexing, Fig. 16 shows the results of 2 layer spatial multiplexing beams in the −20° and +10° directions in the anechoic chamber using OFDM with Notch Out by applying the NPR method.

In Fig. 16, when the above-mentioned spatial multiplexing in the 2 layer beams direction is performed in the high output power region (CFR setting 9.2dB, DPD On, 2 layer beams output level is set to the maximum rated output power +5dB), along with the envelopes of angular spectrum for the desired wave radiation "S" in each two direction and the multitone distorted radiation "I" generated during multiplexing, the angular spectrums for each layer beam are also plotted in Fig. 16. One situation shows that null in +10° direction for the desired radiation "S" set to the −20° direction (upper figure in Fig. 16), and the other situation shows that null in −20° direction for the desired radiation "S" set to the +10° direction (lower figure in Fig. 16). Therefore, in

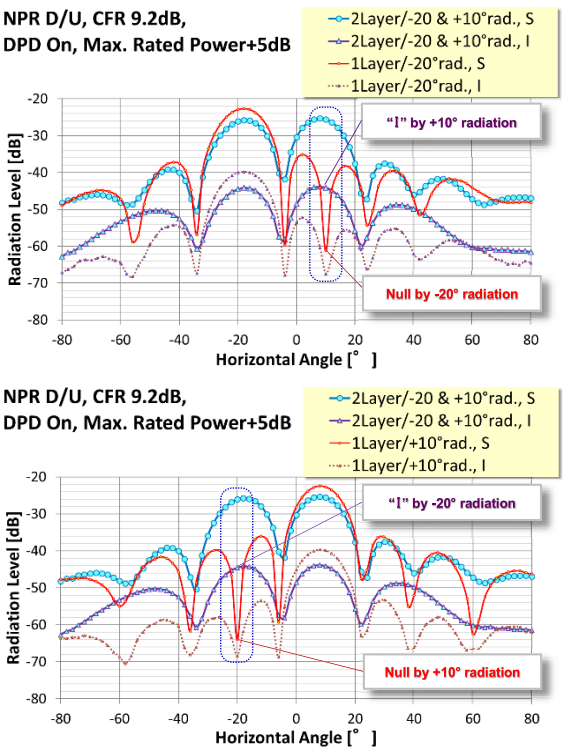

Fig. 16 S/I angular spectrum at −20deg./+10deg. each beam radiation, and level relation between each null and multitone distorted radiation "I"

order to explain the degree of influence of null and nonlinear distorted radiation on spatial multiplexing performance, the pattern aspect for null generated by these two "S" layer beams and the nonlinear distorted radiation pattern "I" occurred by the high output level of each "S" layer beam radiation are given in the same Fig. 16.

During spatial multiplexing in the high output power region as shown in Fig. 16, the multitone distortion component "I", which greatly exceeds null level, is emitted in the same direction as each desired radiation "S", so the DL SINR of each desired wave does not depend on null. Thus, it can be confirmed that the DL SINR performance deterioration under the spatial multiplexing is dominated by "I" degradation caused by the nonlinear distorted radiation.

Consequently, in spatial multiplexing under such a strong nonlinear situation, distortion improvement by installing DPD is very effective as a necessary countermeasure for AAS and DPD is the required measure to be applied.

However, when the nonlinear distortion is improved by DPD and the transmit power is set at a low level, the influence of null accuracy becomes dominant in realizing excellent spatial multiplexing performance with high DL SINR, so it is important to use high precision CAL together.

Therefore, considering the above results, as similar to the AAS verified in this paper, it is very effective to equip AAS with a dual compensation configuration of DPD and high-precision DL CAL. Thus, by applying the above mentioned measures, it is possible to realize AAS with the excellent spatial multiplexing performance, which can maintain high DL SINR during spatial multiplexing over a wide range of TX output power level [4].

7. Conclusions

In this paper, we confirmed the affection of nonlinear distortion in the high TX output power region on spatial multiplexing performance. Since the DL SINR is predominantly determined by radiating the multitone distortion in each user terminal direction during OFDM operation, it is effective to install DPD for each TX in AAS for the improvement of DL SINR.

In addition, the accuracy of null generated in each multiple direction of interfered user terminal does not depend on the degree of nonlinearity and is only affected by the residual amplitude and phase variation between all transmitters and receivers after DL/UL CAL.

Thus, the double compensation configuration of DPD and high-precision DL CAL is very effective in achieving the excellent Massive-MIMO and special multiplex performance.

Acknowledgments

This paper contains some of the results of "Research and Development for the Realization of 5th Generation Mobile Communication Systems", which was commissioned by the Ministry of Internal Affairs and Communications.

References

[1] T. Mochizuki and M. Hirabe, "[Invited Lecture] Development of Low-SHF-Band Massive Element Active Antenna for 5G Mobile and Wireless Communications System," IEICE Society Conference, BCS-1-9, Sept. 2016.
[2] T. Mochizuki, M. Hirabe, M. Hayakawa, and T. Kikuma, "Development of 4.65GHz Band Massive Element Active Antenna for 5G," IEICE General Conference, B-1-119, March 2018.
[3] T. Mochizuki, M. Hirabe, T. Kikuma, M. Hayakawa, and N. Tawa, "[Invited Symposium] Technical Subjects for Essential Circuit Design of Massive Element Active Antenna used for 5G Mobile and Wireless Communications System," IEICE General Conference, CI-3-1, March 2017.
[4] T. Mochizuki, M. Hirabe, T. Kikuma, M. Hayakawa, and D. Nose, "[Symposium Session] Development of 4.65GHz Band Massive Element Active Antenna with Digital Predistortion (DPD) for 5G," IEICE Society Conference, BS-1-3, Sept. 2018.
[5] C. Mollén, U. Gustavsson, T. Eriksson, and E.G. Larsson, "Out-of-Band Radiation Measure for MIMO Arrays with Beamformed Transmission," IEEE Int'l Conference on Comm. 2016 Wireless Comm. Symp., pp.1–6, May 2016.
[6] K. Hausmair, S. Gustafsson, C. Sanchez-Perez, P.N. Landin, U. Gustavsson, T. Eriksson, and C. Fager, ' "Prediction of Nonlinear Distortion in Wideband Active Antenna Arrays," IEEE Trans on Microw. Theory Techn., vol.65, no.11, pp.4550–4563, 2017.
[7] U. Gustavsson, "Power Amplifiers in Advanced Antenna Systems," ISSCC Forum, Circuit and system tech. for mm-wave multi-ant. systems, Feb. 2018.
[8] C. Mollén, E.G. Larsson, U. Gustavsson, T. Eriksson, and R.W. Heath, "Out-of-Band Radiation from Large Antenna Arrays," IEEE Commun. Mag., vol.56, no.4, pp.196–203, 2018.
[9] C. Fager, M. Özen, K. Hausmair, S. Gustafsson, U. Gustavsson, P. Landin, C. Sanchéz-Pérez, J. Chani-Cahuana, and T. Eriksson, "Linear and Efficient Transmitters for Active Antenna Arrays," IEEE Int'l Microw. Symp., WMG-8, June 2018.
[10] A. Prata, J. Sveshtarov, S.C. Pires, A.S.R. Oliveira, and N.B. Carvalho, "Optimized DPD Feedback Loop for m-MIMO sub-6GHz Systems," 2018 IEEE/MTT-S International Microwave Symposium - IMS, pp.485–488, 2018.
[11] H. Masaki and M. Tanaka, "Reduction Method for Intermodulation Interference in Multibeam System using Digital Beamforming," IEICE Society Conference, B-3-8, Sept. 2006.
[12] H. Masaki and M. Tanaka, "Intermodulation Interference Reduction Method with Frequency Reuse in Multi-Beam System using Digital Beamforming," IEICE General Conference, B-3-13, March 2007.
[13] T. May and H. Rohling, "Reduction The Peak-to-Average Ratio in OFDM Radio Transmission Systems," IEEE 48th VTC '98, vol.3, pp.2474–2478, 1998.
[14] Y. Yamao, T. Hamanaka, Y. Ma, K. Tanji, and E. Otobe, "A Simple Digital Predistortion Architecture for Beamforming Transmitter," in PIERS 2015, 1P9-11, Prague, July 2015.
[15] T. Hamanaka, Y. Yamao, Y. Ma, K. Tanji, and E. Otobe, "A Simple DPD for Nonlinear Compensation on Beamforming Transmitter," IEICE Technical Report, MW2015-84, July 2015.
[16] T. Kaho, T. Nakagawa, K. Araki, and K. Horikawa, "Carrier Power to Intermodulation-Distortion Power-Ratio-Increasing Technique in Active Phased-Array Antenna Systems," IEEE Trans. Microw. Theory Techn., vol.50, no.12, pp.2987–2994, 2002.
[17] S. Habu, Y. Yamao, H. Ishikawa, and T. Maniwa, "A Study of DPD Configuration for Beamforming Transmitter," IEICE Technical Report, RCS2018-116, July 2018.
[18] S.A. Bassam, M. Helaoui, and F.M. Ghannouchi, "Crossover Digital Predistorter for the Compensation of Crosstalk and Nonlinearity in MIMO Transmitters," IEEE Trans. Microw. Theory Techn., vol.57, no.5, pp.1119–1128, 2009.

[19] C. Fager, X. Bland, K. Hausmair, J.C. Cahuana, and T. Eriksson, "Prediction of Smart Antenna Transmitter Characteristics Using a New Behavioral Modeling Approach," 2014 IEEE MTT-S International Microwave Symposium (IMS2014), pp.1–4, 2014.
[20] Z. Zhang, Y. Shen, S. Shao, W. Pan, and Y. Tang, "An improved crosstalk cancelling digital predistortion for MIMO transmitters," Mobile Information Systems, vol.2016, pp.1–7, 2016.
[21] S. Hesami, J. Dooley, Ziming, Wang, and R. Farrell, "Digital Predistorter in Crosstalk Compensation of MIMO Transmitters," 2016 27th Irish Signals and Systems Conference (ISSC), pp.1–5, June 2016.
[22] C. Fager, K. Hausmair, K. Buisman, K. Andersson, E. Sienkiewicz, and D. Gustafsson, "Analysis of Nonlinear Distortion in Phased Array Transmitters," 2017 Integrated Nonlinear Microwave and Millimetre-wave Circuits Workshop (INMMiC), pp.1–4, 2017.
[23] N. Tervo, J. Aikio, T. Tuovinen, T. Rahkonen, and A. Parssinen, "Digital Predistortion of Amplitude Varying Phased Array Utilising Over-the-Air Combining," 2017 IEEE MTT-S International Microwave Symposium (IMS), pp.1165–1168, 2017.
[24] K. Hausmair, P.N. Landin, U. Gustavsson, C. Fager, and T. Eriksson, "Digital Predistortion for Multi-Antenna Transmitters Affected by Antenna Crosstalk," IEEE Trans. Microw. Theory Techn., vol.66, no.3, pp.1524–1535, 2018.
[25] K. Hausmair, U. Gustavsson, C. Fager, and T. Eriksson, "Modeling and Linearization of Multi-Antenna Transmitters Using Over-the-Air Measurements," 2018 IEEE International Symposium on Circuits and Systems (ISCAS), pp.1–4, 2018.
[26] T. Mochizuki, M. Hirabe, T. Kikuma, M. Hayakawa, and D. Nose, "[Invited Lecture] A study of the Specificity of Nonlinear Distortion Radiation in Multitone Transmission using 4.65GHz Band Massive Element Active Antenna System for 5G," IEICE Technical Report on Technical Committee on Antennas and Propagation, A·P 2018-178, Feb. 2019.
[27] Y. Saito, A. Benjebbour, Y. Kishiyama, X. Wang, X. Hou, H. Jiang, L. Lu, B. Li, W. Liang, L. Gu, Y. Cui, and T. Kashima, "Investigation on the Performance of TDD Massive MIMO in the 4.5GHz Band," IEICE Technical Report, Radio Communication System, vol.116, no.396, RCS2016-240, pp.25–30, Jan. 2017.
[28] H. Wei, D. Wang, H. Zhu, J. Wang, S. Sun, and X. You, "Mutual coupling calibration for multiuser Massive MIMO systems," IEEE Trans. Wireless Commun., vol.15, no.1, pp.606–619, 2016.
[29] D. Jitsukawa, T. Seyama, T. Kobayashi, T. Oyama, T. Dateki, H. Seki, and M. Minowa, "Study of Inter-Transmission Point Calibration Scheme for 5G Ultra High-Density Distributed Antenna Systems," IEICE Technical Report, RCS2016-142, pp.71–76, Aug. 2016.
[30] T. Takagi, S. Ogura, Y. Ikeda, and N. Suematsu, "Intermodulation and Noise Power Ratio Analysis of Multiple-Carrier Amplifiers Using Discrete Fourier Transform," IEICE Trans. Electron., vol.E77-C, no.6, pp.935–941, June 1994.
[31] M. Nakayama and T. Takagi, "Distortion Calculation method of Micro Wave Amplifier," Mitsubishi Electric Technical Report, vol.71, no.10, pp.69–71, 1997.

Takuji Mochizuki received the B.S. degrees in Electrical Engineering from Keio University in 1983. Jointed NEC Corporation in the same year and he has been engaged in the development of mobile satellite base stations, wireless LAN Access Point, mobile terminal, UWB LSIs and mobile base station. Currently engaged in Active Antenna System for 5G as Advanced Technologist in NEC Certified Professional. He is a member of the Institute of Electronics, Information and Communication Engineers (IEICE) in Japan.